Assessment on the Use of High Capacity "Sn$_4$P$_3$"/NHC Composite Electrodes for Sodium-Ion Batteries with Ether and Carbonate Electrolytes

Thangavelu Palaniselvam,* Charan Mukundan, Ivana Hasa, Aggunda L. Santhosha, Mustafa Goktas, Hyein Moon, Mirco Ruttert, Richard Schmuch, Kilian Pollok, Falko Langenhorst, Martin Winter, Stefano Passerini, and Philipp Adelhelm*

This work reports the facile synthesis of a Sn–P composite combined with nitrogen doped hard carbon (NHC) obtained by ball-milling and its use as electrode material for sodium ion batteries (SIBs). The "Sn$_4$P$_3$"/NHC electrode (with nominal composition "Sn$_4$P$_3$":NHC = 75:25 wt%) when coupled with a diglyme-based electrolyte rather than the most commonly employed carbonate-based systems, exhibits a reversible capacity of 550 mAh g$_{electrode}^{-1}$ at 50 mA g^{-1} and 440 mAh g$_{electrode}^{-1}$ over 500 cycles (83% capacity retention). Morphology and solid electrolyte interphase formation of cycled "Sn$_4$P$_3$"/NHC electrodes is studied via electron microscopy and X-ray photoelectron spectroscopy. The expansion of the electrode upon sodiation (300 mAh g$_{electrode}^{-1}$) is only about 12–14% as determined by in situ electrochemical dilatometry, giving a reasonable explanation for the excellent cycle life despite the conversion-type storage mechanism. In situ X-ray diffraction shows that the discharge product is Na$_{15}$Sn$_4$. The formation of mostly amorphous Na$_3$P is derived from the overall (electro)chemical reactions. Upon charge the formation of Sn is observed while amorphous P is derived, which are reversibly alloying with Na in the subsequent cycles. However, the formation of Sn$_4$P$_3$ can be certainly excluded.

1. Introduction

Sodium-ion batteries (SIBs) are electrochemical energy storage systems aiming at complementing the lithium-ion and lead-acid battery technologies in mobile and grid storage applications.[1] Considerable progress has been achieved in just a few years, however, to achieve the commercialization of SIBs in practical application, further improvement is needed. Thus, the design and the optimization of electrode materials characterized by improved capacity and cycle life are of great importance. Graphite is the state-of-the-art anode for LIBs, yet its use in SIBs is limited so far due to the lack of thermodynamically stable, sodium-rich graphite intercalation compounds (GICs) Na$_x$C.[2] An exception is found for ether-based electrolytes in which solvated sodium-ions can reversibly intercalate into the graphite lattice.[3] The obtained capacity of 110 mAh g^{-1}, however, is too low for high energy density application and would restrict its use to high power devices.[4] Higher storage capacities can be achieved using other, disordered forms of carbon, which can be produced from various precursors such as pitch, gas, or biomaterials.[5] Depending on their local structure most of these materials can be classified as either hard or soft carbon. The Na$^+$ storage capacity is typically ranging between 200 and 350 mAh g$^{-1[6–15]}$ though also values

Dr. T. Palaniselvam, C. Mukundan, A. L. Santhosha, Dr. M. Goktas, Prof. P. Adelhelm
Institute of Technical Chemistry and Environmental Chemistry
Friedrich Schiller University Jena
Philosophenweg 7a, Jena 07743, Germany
E-mail: thangavp@hu-berlin.de; philipp.adelhelm@hu-berlin.de
Dr. T. Palaniselvam, A. L. Santhosha, Dr. M. Goktas, Prof. P. Adelhelm
Department of Chemistry
Humboldt-University of Berlin
Brook-Taylor Str. 2, Berlin 12489, Germany

The ORCID identification number(s) for the author(s) of this article can be found under https://doi.org/10.1002/adfm.202004798.

Dr. I. Hasa, H. Moon, Prof. S. Passerini
Helmholtz Institute Ulm (HIU)
Helmholtzstrasse 11, Ulm 89081, Germany
Dr. I. Hasa, H. Moon, Prof. S. Passerini
Karlsruhe Institute of Technology (KIT)
P.O. Box 3640, Karlsruhe 76021, Germany
M. Ruttert, Dr. R. Schmuch, Prof. M. Winter
MEET Battery Research Center
University of Muenster
Corrensstr. 46, Münster D-48149, Germany
Dr. K. Pollok, Prof. F. Langenhorst
Institute of Geosciences
Friedrich Schiller University Jena
Carl-Zeiss-Promenade 10, Jena 07745, Germany
Prof. M. Winter
Helmholtz Institute Münster
IEK-12
Forschungszentrum Jülich GmbH
Corrensstr. 46, Münster 48149, Germany

ADVANCED
SCIENCE NEWS
www.advancedsciencenews.com

ADVANCED
FUNCTIONAL
MATERIALS
www.afm-journal.de

exceeding 400 mAh g^{-1} have been reached by high temperature treatment.[16] However, a potential roadblock is that much of the sodiation occurs close to the metal plating potential, which compromises safety. The capacity of disordered carbons under practical conditions might be therefore not sufficient. Another challenge is that many disordered carbons suffer from a low initial Coulomb efficiency (ICE) due to side reactions leading to solid electrolyte interphase (SEI) formation and irreversible trapping of sodium ions.

Research on tin (Sn) and phosphorous (P) based anodes is largely motivated by their high theoretical Na storage capacity[17,18] through formation of Na$_{15}$Sn$_4$ (theoretical capacity q_{th} = 847 mAh g^{-1}) and Na$_3$P (q_{th} = 2560 mAh g^{-1}) in a alloying reaction, respectively.[19,20] The combination of both elements in tin phosphide (Sn$_4$P$_3$, q_{th} = 1132 mAh g^{-1}) has been studied as potential anode material for SIBs as well.[21] Upon sodiation, Sn$_4$P$_3$ undergoes a conversion type reaction, providing high gravimetric and volumetric capacity with an average working potential of around 0.3 V versus Na$^+$/Na, thus potentially enabling cells with high theoretical energy density.[22] On the downside, it is well known that conversion reactions typically exhibit a large voltage hysteresis and large volume changes, e.g., 420% and 490% for formation of Na$_{15}$Sn$_4$[23] and Na$_3$P[24] respectively. Expansion and shrinkage of the electrode during cycling ("breathing") is generally linked to unstable interfaces, particles contact loss, and hence poor cycle life. Nanosizing and embedding Sn and P in suitable matrixes have been effective strategies to mitigate some of the mentioned issues, however not to the required level. In the specific case of Sn$_4$P$_3$, the poor electronic conductivity is an additional limitation, which again up to now has been generally addressed by adding carbon[25–27] or TiC as additive.[28] Despite the slight improvement in cycle life, in many cases, stable cycling could not be achieved over more than 150 cycles, so further improvement is needed.

A valid strategy to improve the cycle life of electrode materials is a rational design of the electrolyte solutions, especially with respect to the SEI. Carbonate-based electrolytes are the most commonly employed solutions for Sn$_4$P$_3$. Table S1 in the Supporting Information reports a comparison of the electrochemical performance of Sn$_4$P$_3$ based composite electrodes existing in the literature. High capacities in the range of ≈500–900 mAh g$^{-1}_{Sn-P}$ are reported, however with limited cycle life. The use of fluoroethylene carbonate (FEC) as electrolyte additive has shown to improve cycle life although it is known that FEC is prone to lead to the formation of a more resistive SEI, which is detrimental to the electrochemical performance.[29,30] Sakaguchi et al. reported an improvement of the ICE in the first cycle when using an ionic liquid-based electrolyte. Indeed, when employing a *N*-methyl-*N*-propylpyrrolidinium bis(fluorosulfonyl)amide (Py13-FSA) based electrolyte, the ICE value reached 78% compared to 54% obtained for a propylene carbonate (PC)-based electrolyte.[31] However, the same electrode failed to show stable cycling for more than 50 cycles. Overall, it is clear that the electrolyte strongly affects the cycling behavior of Sn$_4$P$_3$ electrodes in sodium-ion cells and that there is a need for optimized salt/solvents combinations enabling stable cycling and high practical capacities.

Very recently, ether-based electrolytes have been more widely investigated for graphite,[32] hard carbon,[33] Bi,[34,35] and Sn based electrodes[36,37][17] due to their generally enhanced compatibility with many anode materials (Sb being an exception[36]). Note that the stability of the electrolyte is also depending on the type of conductive salt used with sodium trifluoromethanesulfonate (NaOTf) and NaPF$_6$ being clearly favored (at least in half-cell experiments).[38] The use of a glyme-based electrolyte for Sn$_4$P$_3$ electrodes in SIBs has been suggested only very recently by Gómez-Cámer et al.[39] A capacity of 900 mAh g^{-1} with an ICE value of ≈90% was reported, however the capacity dropped to 388 mAh g^{-1} after 100 cycles (43% of capacity retention). The same report also disclosed that when coupling the Sn$_4$P$_3$-based anode with a glyme-based electrolyte, superior performance was achieved compared to carbonate-based ones, especially in terms of specific capacity and coulomb efficiency. The beneficial properties of glyme-based electrolytes have been also reported for TiO$_2$ anodes,[40] and have been attributed to the formation of a less resistive SEI.[41] A similar understanding is lacking so far in the case of Sn$_4$P$_3$. Moreover, although it is known that the reaction of Na with Sn$_4$P$_3$ involves the formation of several Na–Sn and Na–P intermediate phases,[42] the overall understanding of the reaction is still poor. X-ray diffraction (XRD) studies have been performed in order to investigate the sodiation mechanism, however only limited information can be gained due to partial amorphization but the formation of different sodiated phases has been reported.[43] Obrovac et al. proposed Na$_3$P, Na$_5$Sn$_2$ and Na$_{15}$Sn$_4$ as the possible discharge products,[44] while Yang et al. found Na$_3$P and Na$_{15}$Sn$_4$ as the discharge products.[42] In some cases, XRD reflections including the ones of Sn and P could not be detected after desodiation.[45] Overall, the analysis is also hampered by the fact that intermediate Na–P and Na–Sn phases produced upon cycling are easily hydrolyzed or oxidized during sample preparation or/and transfer for post-mortem analysis.[46] In this scenario, the use of in situ methods becomes a very useful strategy.

Herein, we study the properties of a composite anode material containing Sn$_4$P$_3$ as main active material and nitrogen doped hard carbon (NHC) as support. NHC has been selected due to the proven beneficial effect of N-doping on the electronic conductivity of carbon matrices, which translates in the improved electrochemical performance, including cycle life, as comprehensively described in literature.[17][47] The preparation of the composite material is done by ball milling Sn$_4$P$_3$ and NHC. The preparation method leads to a phase mixture containing Sn$_4$P$_3$, beta Sn, amorphous P, and NHC, which is hence defined as "Sn$_4$P$_3$"/NHC (instead of stoichiometric Sn$_4$P$_3$/NHC) with an overall composition of "Sn$_4$P$_3$":NHC = 75:25 wt%. In combination with the diglyme electrolyte a capacity of 550 mAh g$_{electrode}^{-1}$ at 50 mA g^{-1} and 440 mAh g$_{electrode}^{-1}$ over 500 cycles (83% of capacity retention) is obtained being a notable improvement compared to previous studies (contributions of the NHC and the conductive additive being shown to be negligible). More information on the storage behavior is obtained from in situ electrochemical dilatometry and in situ XRD. Moreover, XPS is applied to study the surface film formation. Overall, the present work reveals several aspects for the improved electrochemical performance of "Sn$_4$P$_3$" for SIBs in ether-based electrolytes.
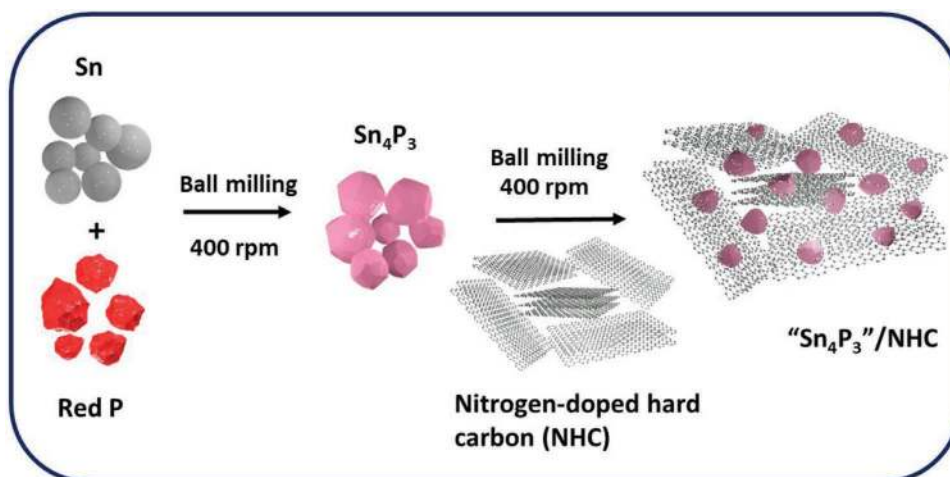
Scheme 1. Sketch of the synthesis path of "Sn$_4$P$_3$"/nitrogen doped hard carbon (NHC). The nominal composition (wt%) of the composite is "Sn$_4$P$_3$": NHC = 75:25 wt%.

2. Results and Discussion

2.1. Synthesis and Structural Characterization

The Sn$_4$P$_3$ composite was prepared by simple ball milling of Sn powder and red P in Ar atmosphere. The resulting powder was then ball milled with nitrogen-doped hard carbon (NHC) (75:25 wt%) to produce the "Sn$_4$P$_3$"/NHC composite (**Scheme 1**). NHC was prepared by annealing chitosan at 1100 °C under Ar atmosphere. The detailed experimental method is described in the Supporting Information.

Figure 1 shows transmission electron microscopy (TEM) images of the "Sn$_4$P$_3$"/NHC composite. The composite consists of irregularly shaped submicrometric agglomerates of nanoparticles. Lattice fringes of Sn$_4$P$_3$ (107)[48] in Figure 1d and the electron diffraction information (Figure 1e,f) from main diffraction rings corresponding to Sn$_4$P$_3$ and document its crystallinity. In the XRD pattern of the "Sn$_4$P$_3$"/NHC composite (discussed in later section) Sn$_4$P$_3$ and Sn were identified as crystalline phases which indicated that the Sn$_4$P$_3$ phase within the "Sn$_4$P$_3$"/NHC composite was partially disproportionated to Sn and P (amorphous) as a result of the high energy ball milling process. The electron diffraction information is compatible with this as Sn shows lattice spacing that are very close to those of Sn$_4$P$_3$. The TEM images do not show clear regions of NHC suggesting that NHC and Sn$_4$P$_3$ were homogeneously mixed with each other. This is corroborated from STEM-EDX elemental mapping (**Figure 2**), which shows an overlapping distribution of carbon with Sn and P on sub-micrometer scale.

The as synthesized material has also been characterized by XRD and XPS. The NHC shows the two very broad (002) and (101) reflections, respectively at around $2\theta = 25°$ and 45° due to the presence of small graphene domains and their local ordering (Figure S1, Supporting Information). Similarly, red P shows a weak broad reflection due to the (013) planes (Figure S1, Supporting Information).[49] Figure S1 (Supporting Information) (blue curve) and **Figure 3**a shows the XRD pattern of Sn$_4$P$_3$, which shows a series of defined reflections. All XRD reflections can be indexed to the Sn$_4$P$_3$ phase (Pearson's number-1910451) based on the hexagonal space group of *R*-3*m*,[50] which is in accordance

to previous results (Table S1, Supporting Information).[43] In "Sn$_4$P$_3$"/NHC, i.e., after ball milling of Sn$_4$P$_3$ with NHC, some Sn$_4$P$_3$ converted to beta-Sn (Pearson's number-1819724) and

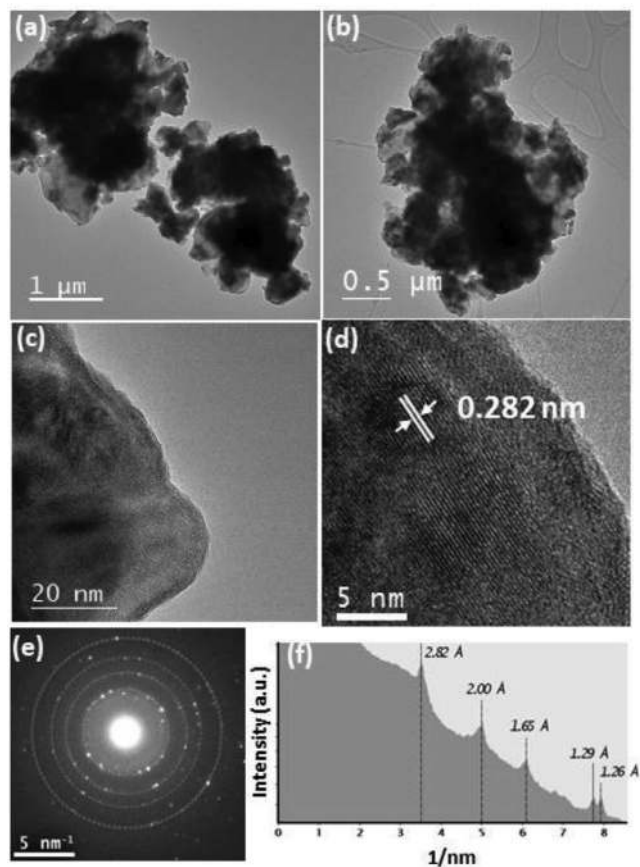**Figure 1.** a–c) TEM images of "Sn$_4$P$_3$"/NHC at different magnifications. d) High-resolution TEM image showing (107) lattice fringes of Sn$_4$P$_3$. e) Selected area electron diffraction (SAED) from "Sn$_4$P$_3$"/NHC. The rings mark the positions of selected strong reflections from Sn$_4$P$_3$ that are well displayed in an f) integrated average intensity profile calculated from the diffraction ring pattern.
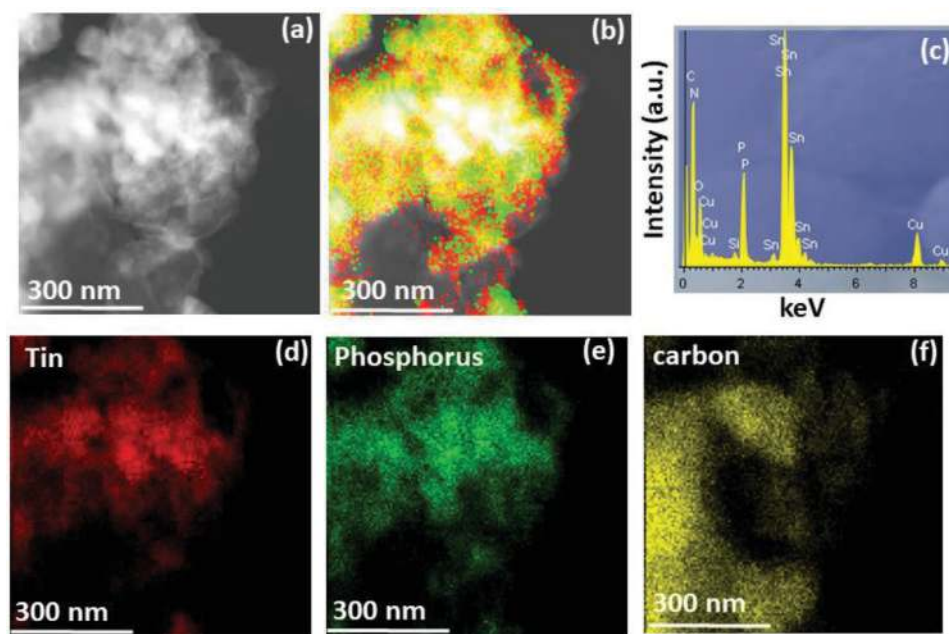
**ADVANCED
SCIENCE NEWS**

www.advancedsciencenews.com

**ADVANCED
FUNCTIONAL
MATERIALS**

www.afm-journal.de

Figure 2. a) STEM-HAADF image and b) EDX mapping of "Sn_4P_3/NHC" showing the overlapping distribution of tin, phosphorous and carbon. c) EDX spectra with corresponding elemental mapping of d) tin, e) phosphorous and f) carbon.

amorphous P (see Figure 3b). However, the reflections corresponding to amorphous red P could not be distinguished clearly. The average crystallite sizes were estimated by the Scherrer equation to be ≈12 nm for Sn_4P_3 and 16 nm for "Sn_4P_3"/NHC.

To study the chemical environment of Sn, XPS was carried out for "Sn_4P_3"/NHC. The survey spectrum presented in Figure S2a (Supporting Information) provides clear indication of the presence of carbon (C), nitrogen (N), tin (Sn), phosphorous (P), and oxygen (O) in the active composite, without any additional impurity. The deconvoluted spectrum of the Sn 3d region (Figure S2b, Supporting Information) shows a pair of peaks at 486.5 eV (Sn $3d_{5/2}$) and 495.2 eV (Sn $3d_{3/2}$) for Sn^{4+}, indicating a Sn–O environment.[51] A peak at 484.3 eV is likely due to Sn^0 and/or Sn_4P_3, which shows a metallic Sn-like bonding.[52] In addition, a peak at 492.1 eV corresponding to Sn bound with P, indicating the coordination of Sn with P in Sn_4P_3 phase. Accordingly, the P 2p spectrum (Figure S2c, Supporting Information) shows a peak at 128.3 eV corresponding to P coordinated with Sn.[52] The additional peaks at 132.1 and 137.4 eV can be assigned to P bonding with carbon (C_3-P groups)[53] or some surface oxygen functional groups and Sn 4s electrons.[54] Meanwhile, the nitrogen doping in NHC was confirmed from the deconvoluted N 1s spectrum (Figure S2d, Supporting Information). The nitrogen atoms are predominantly existing as graphitic nitrogen (400.6 eV). Overall, it can be concluded that some fractions of Sn_4P_3 are converted into Sn and amorphous P due to the high-energy ball milling process resulting in a mixture of Sn_4P_3, Sn and P phases in the "Sn_4P_3"/NHC active composite.

2.2. Electrochemical Characterization of "Sn_4P_3"/NHC

The sodium storage behavior of "Sn_4P_3"/NHC was evaluated by galvanostatic discharge/charge experiments at 50 mA g^{-1} (**Figure 4**). 1 M $NaPF_6$ in diglyme (2G) was employed as electrolyte.

The electrode exhibits an initial discharge capacity around 815 mAh $g_{electrode}^{-1}$ (see **Table 1**) and an ICE of 67.5% (Figure 4a). The index electrode indicates that the capacity was normalized on the mass of the electroactive components of the electrode, i.e., "Sn_4P_3" (62.5 wt%), NHC (20.8 wt%) and Super P (16.7 wt%). The low ICE is a combined effect of electrolyte decomposition (SEI formation), and irreversible trapping of Na ions in NHC and the conductive additive. As the composite shows only a low BET surface area of ≈3 m^2 g^{-1} (Figure S3, Supporting Information), excessive SEI formation due to a large absolute surface area can be excluded. More relevant is the irreversible Na trapping in the carbon-based components of the electrode. NHC and Super P as individual components exhibit ICE values as low as 54% and 26%, respectively, when cycled under identical conditions, see Figure S4 (Supporting Information).

Immediate stabilization of the electrode took place from the second cycle on. The second cycle capacity was 550 mAh $g_{electrode}^{-1}$ with 99.9% Coulomb efficiency. 550 mAh $g_{electrode}^{-1}$ corresponds to 65% of the theoretical capacity of the composite electrode (842 mAh $g_{electrode}^{-1}$, see calculation in the Supporting Information), which indicates that the conversion reaction is incomplete. As NHC and Super P can contribute with 212 mAh g_{NHC}^{-1} and 180 mAh $g_{Super P}^{-1}$ at maximum (Figure S4, Supporting Information), their contribution to the capacity in the composite (at second cycle) is lower than 10% (see Supporting Information), i.e., most of the capacity is due to "Sn_4P_3."

Compared to the previously reported values for Sn_4P_3/C electrodes (500–900 mAh g^{-1}, Table S1, Supporting Information), the capacity of "Sn_4P_3"/NHC (550 mAh $g_{electrode}^{-1}$) used in this work is lower, which can be related to the high carbon content. The obtained specific capacity for "Sn_4P_3"/NHC can be attributed to the formation of Sn–Na ($Na_{14}Sn_4$) and Na-P (Na_3P)
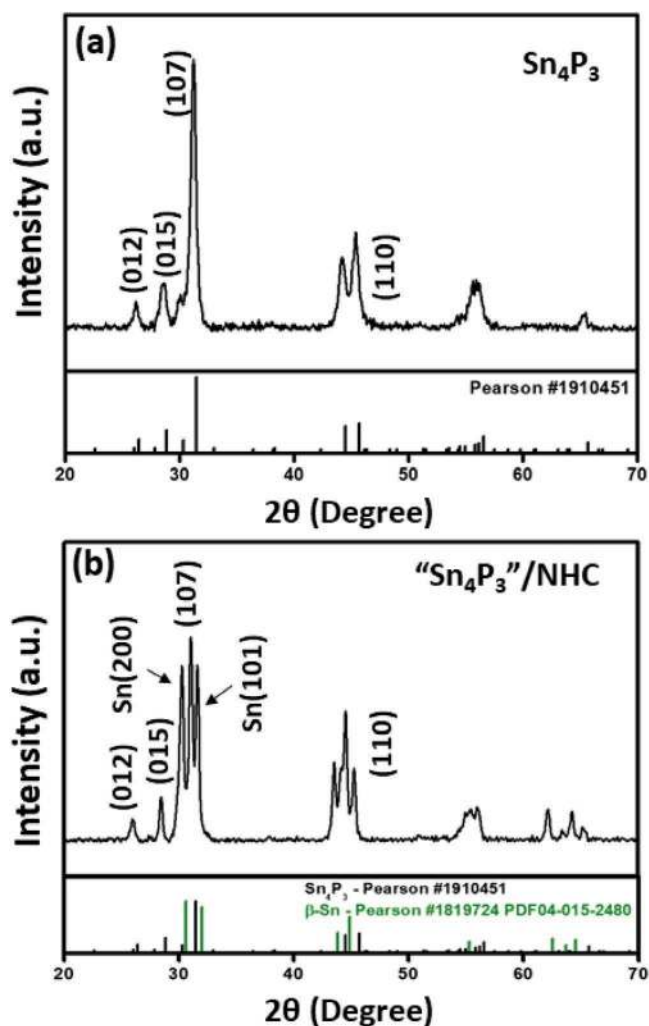
Figure 3. a) XRD pattern of Sn_4P_3 and b) XRD pattern of "Sn_4P_3"/NHC (showing also some Sn reflections).

compounds. In fact, the shape of the voltage profile is a direct indication of the storage mechanism. Well-defined plateaus are expected to appear for $Na_{14}Sn_4$ particularly in desodiation, while a very sloping profile over the whole voltage window is found for "Sn_4P_3"/NHC. Such sloping behavior is characteristic for disordered carbon and phosphorous, which do not possess crystallinity. Although, reflections corresponding to the intermetallic phases of $Na_{14}Sn_4$ are clearly visible during sodiation/desodiation by in situ XRD that is discussed in the later section. Overall, the voltage profile indicates that several simultaneous processes occur during Na storage and release.

To illustrate the benefit of the diglyme-based electrolyte, the cycling experiments were carried out with carbonate-based electrolytes using solvent mixtures of EC:PC (1:1 vol%) as well as EC:PC:FEC (2% vol). The results are compared in Figure 4b. The storage capacity with diglyme (550 mAh $g_{electrode}^{-1}$) is significantly higher compared to when EC:PC (407 mAh $g_{electrode}^{-1}$) or EC:PC: FEC (358 mAh $g_{electrode}^{-1}$) are used. In general, ether-based electrolytes provide a stable and favorable SEI,[55] hence facilitating the charge transfer and storage processes.[56] As shown in Figure 4b, the charging of the cells with carbonate

electrolytes occurs at higher voltages compared to when the diglyme electrolyte is used. Such a higher overpotential suggests that the resistance is larger when carbonate electrolytes are used. This can be directly seen from the offset of around 100 mV at the beginning of charging for the cells with carbonate electrolytes, see Figure 4b, and is supported by electrochemical impedance spectroscopy (EIS). Figure S5 (Supporting Information) shows impedance spectra upon cycling in the frequency range of 1 MHz to 10 mHz of two-electrode cells cycled in both the electrolytes. While for the cell cycled in carbonate electrolyte a higher electrolyte conductivity is observed (7.4 Ω compared to 12.1 Ω for the diglyme-based electrolyte), the overall impedance over the probed frequency range is notably higher for the cell cycled in the carbonate-based electrolyte, which further increases upon cycling (a decrease is instead observed for the diglyme-based electrolyte). In the two-electrode cell set up, it is worth mentioning that the sodium metal counter electrode strongly impacts the overall impedance, however, the results clearly show that the use of the diglyme electrolyte leads to a much more favorable, i.e., less resistive and more stable SEI.

The cycle life of "Sn_4P_3"/NHC was also studied with different electrolytes. Figure 4c shows the results for the EC:PC based electrolyte with and without FEC additive and the glyme based system at 500 mA g^{-1} over 300 and 500 cycles, respectively. The higher specific capacity was obtained using EC:PC reaching 456 mAh $g_{electrode}^{-1}$ in the second cycle. However, rapid capacity fading is observed reaching 25 mAh g^{-1} after 20 cycles. The voltage profile of the 100th cycle is reported in Figure S6 (Supporting Information), suggesting carbon super P as the only active material while "Sn_4P_3" being inactive. Komaba et al. showed that FEC as additive can improve the cycle life for Sn and hard carbon-based electrodes by providing a more stable SEI.[18a] Using 2% of this additive, the capacity was much lower (299 mAh $g_{electrode}^{-1}$, second cycle) as compared to the pure EC:PC electrolyte (456 mAh $g_{electrode}^{-1}$). The stability, however, was greatly improved leading to 183 mAh $g_{electrode}^{-1}$ after 500 cycles, i.e., retaining 61.2% of its capacity.

The by far best results were obtained for the diglyme electrolyte with 535 mAh $g_{electrode}^{-1}$ delivered in the second cycle. After 500 cycles, the composite electrode shows a specific capacity of 440 mAh $g_{electrode}^{-1}$, i.e., 83% of capacity retention. In our experiments, the cycling stability of Sn_4P_3 (with Super P) and NHC was also studied separately using 1 M $NaPF_6$ in diglyme as an electrolyte. Due to the absence of NHC, Sn_4P_3 initially shows a higher capacity (897 mAh g_{Sn4P3}^{-1}) than "Sn_4P_3"/NHC (731 mAh $g_{"Sn4P3"}^{-1}$), see **Figure 5**a.

However, a rapid capacity fading was observed for the former (Figure 5b), with almost all the capacity loss occurring within a few cycles. This attribution is due to poor conductivity of Sn_4P_3, evidencing the need for hard carbon in the active composite for achieving stable cycling. Under the same conditions, NHC shows stable cycling with 134 mAh g_{NHC}^{-1} being obtained after 500 cycles with a total capacity retention of 85%. However, the overall capacity for NHC (134 mAh g_{NHC}^{-1}) is low as compared to "Sn_4P_3"/NHC (731 mAh $g_{"Sn4P3"}^{-1}$) and Sn_4P_3 (897 mAh g_{Sn4P3}^{-1}) electrodes (Figure 5a). The rate capability of the "Sn_4P_3"/NHC electrode in the diglyme electrolyte was studied between 50 mA g^{-1} to 2 A g^{-1} for five cycles each, see Figure S7 (Supporting Information). Up to 1 A g^{-1}, the storage capacities
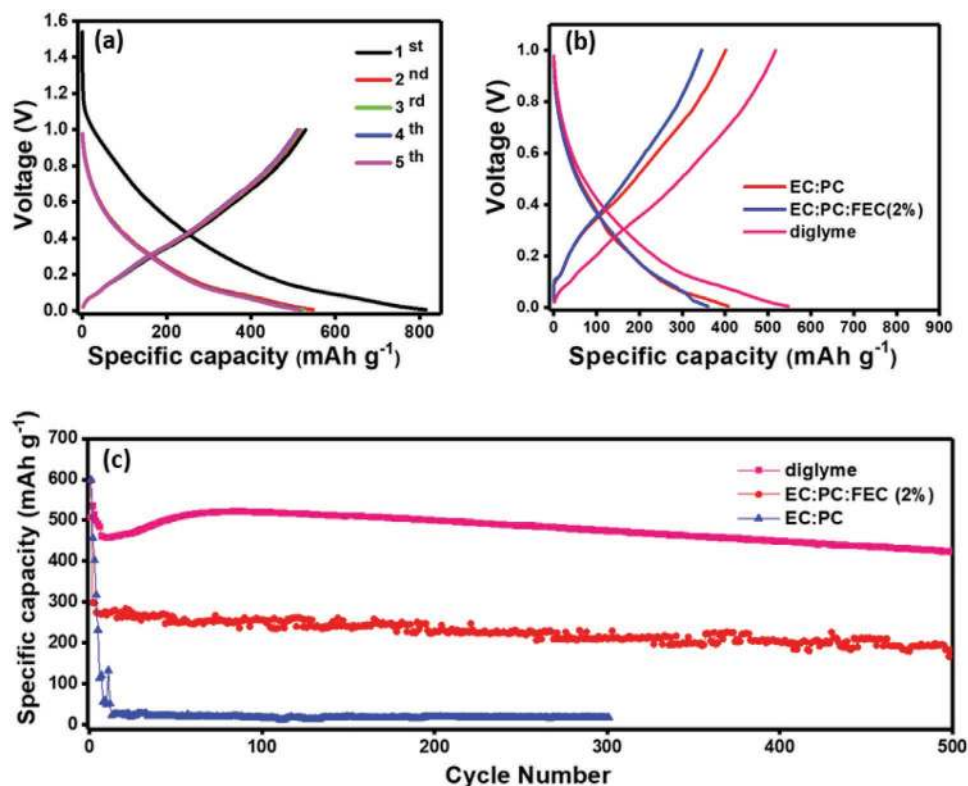
**ADVANCED
SCIENCE NEWS**
www.advancedsciencenews.com

ADVANCED
**FUNCTIONAL
MATERIALS**
www.afm-journal.de

Figure 4. a) Charge–discharge curves of "Sn$_4$P$_3$"/NHC measured at 50 mA g^{-1} using a diglyme-based electrolyte. b) Charge–discharge curves (second cycle) recorded at 50 mA g^{-1} in different electrolyte solutions. c) Cycling stability evaluated with charge/discharge rates of 500 mA g^{-1} for 500 cycles using different electrolytes. All measurements were conducted in two-electrode cells using Na metal as with Na metal as counter electrode. NaPF$_6$ (1 M) was used as conductive salt in all cases. Capacity values refer to all active components of the electrode ("Sn$_4$P$_3$," NHC, and Super P).

exceeded 400 mAh g$_{electrode}$$^{-1}$. At 2 A g^{-1} still 287 mAh g$_{electrode}$$^{-1}$ were obtained. Finally, when the current was reversed back to 50 mA g^{-1}, the discharge capacity recovered its starting value of around 520 mAh g$_{electrode}$$^{-1}$, demonstrating an excellent stability.

2.3. Postmortem Analysis of "Sn$_4$P$_3$"/NHC Electrodes

The improved performance of the "Sn$_4$P$_3$"/NHC electrode in diglyme electrolyte can be understood by analyzing the SEI and the morphology. SEM (Figure S8, Supporting Information) was used to study the overall morphology of the electrodes cycled in diglyme and in EC:PC:FEC electrolytes at 500 mA g^{-1} for 50 cycles. Subsequently the electrodes were recovered in the desodiated state and washed to remove electrolyte residuals.

As can be seen in Figure S8c–f (Supporting Information), both cycled electrodes contain large amounts of polymeric surface deposits (brighter areas). In case of the diglyme electrolyte (Figure S8c,d, Supporting Information), these are more homogenously distributed, forming a continuous film covering the particles. In contrast, the surface morphology is much more inhomogeneous for the electrode cycled in carbonate-based electrolyte (Figure S8e,f, Supporting Information). Note that also the pristine electrode shows some minor polymer deposits which are ascribed to the presence of the PVDF binder, see Figure S8b (Supporting Information). The content, however, is much smaller. The formation of a thick surface films on conversion electrodes is a well-known phenomenon. The thickness of these films can easily reach several nanometers (200 nm) µm as shown in a previous study on CuO thin films (200 nm).[57]

Table 1. Composition of the "Sn$_4$P$_3$"/NHC electrode and contribution of the different components. The theoretical capacity of NHC and Super P was separately determined, see Supporting Information, and assumed to remain stable during cycling. All contributions were normalized according to their weight fraction.

Active components in electrode	Weight content [%]	Theoretical capacity [mAh g^{-1}]	Discharge capacity at first cycle [mAh g^{-1}]	Discharge capacity at second cycle [mAh g^{-1}]
"Sn$_4$P$_3$" (i.e., Sn$_4$P$_3$ + beta-Sn + amorphous P)	62.5	708	741	476
NHC	20.8	44	44	44
Super P	16.7	30	30	30
Total	100	782	815	550

2004798 (6 of 12)

Figure 5. a) Charge–discharge curves (second cycle) of "Sn_4P_3"/NHC, Sn_4P_3, and NHC measured at 50 mA g^{-1} in 1 M NaPF$_6$ in diglyme electrolyte. b) Cycle life test for "Sn_4P_3"/NHC, Sn_4P_3, and NHC electrodes at 500 mA g^{-1} for 500 cycles using in 1 M NaPF$_6$ in diglyme as electrolyte. (The capacity for "Sn_4P_3"/NHC, have represented against the total content of "Sn_4P_3").

Although (from a classical point of view) the SEI is expected to be only a few nm thick, these surface films fulfill a similar function and are therefore often also referred to as SEI.

To get more insights about the composition of the SEI, XPS was carried out. **Figure 6** shows the C 1s spectra of "Sn_4P_3"/NHC electrodes before and after cycling. The bare electrode shows the peaks at 284.9, 286.6, and 288.1 eV corresponding to C−C/C−H groups, i.e., graphitic carbon and hydrocarbons, C−O or C−N and functionalized carbons, respectively. After cycling with diglyme electrolyte an additional peak at 289.0 eV was found, corresponding to sodium alkoxide (RCH$_2$ONa), which is believed to be a main SEI product, i.e., a reduction product of the diglyme electrolyte.[42] In case of the EC:PC:FEC electrolyte, along with the peak corresponding to RCH$_2$ONa, another peak at 291.0 eV was observed that can be attributed to Na$_2$CO$_3$/ROCO$_2$Na, which are the reduced products of the carbonates. The O1s spectrum (Figure 6b) for electrodes cycled in diglyme shows a dominant peak at 532.6 eV corresponding again to RCH$_2$ONa (or more generically to R–O–Na). The peak at 534.4 eV corresponds to a mixture of carbonates and alkylcarbonates, i.e., Na$_2$CO$_3$/ROCO$_2$Na indicating that the SEI contains a mixture of organic and inorganic compounds. In case of EC:PC:FEC, the O1s spectrum also shows signals corresponding to RCH$_2$ONa and Na$_2$CO$_3$/ROCO$_2$Na. The intensity of the latter is however larger, indicating that these compounds form the dominant phase in the SEI. The Na 1s spectrum cycled in both diglyme, carbonate-electrolytes (Figure 6c) shows a peak

at 1072.3 eV, and F 1s spectrum (Figure S9, Supporting Information) showed a peak at 684.9 eV indicating the presence of Na–F and other sodium compounds including RCH$_2$ONa and Na$_2$CO$_3$. In Sn 3d spectrum (Figure 6d), a peak corresponding to the Na auger lines (498.5 eV) can be seen only with cycled electrodes, indicating the existence of Na based products after cycling, while the main features of Sn observed for the pristine electrode disappear upon cycling indicating the formation of a layer hindering the detection of the electrode's surface.

According to the C 1s and O 1s spectral regions, the organic SEI products, i.e., RCH$_2$ONa, ROCO$_2$Na, and inorganic SEI products, i.e., Na$_2$CO$_3$, NaF (with marginal intensity) can be detected in both cases. In the case of the electrode cycled with EC:PC:FEC electrolyte, the amount of inorganic SEI products is higher. It has been reported that sodium alkoxides (RCH$_2$ONa) enhance the Na$^+$ transport and are essential for the interfacial stability in the case of a Bi electrode.[58] On the other hand, Wang et al. have theoretically shown that an ether-based solvent reduces the energy barrier for Na-ion diffusion and therefore increases the electrochemical performances.[59] It is reasonable to assume that the organic SEI products, i.e., sodium alkoxides, also reduce the energy barrier for Na-ion diffusion. Overall, the improved behavior for the diglyme electrolyte is rooted in the lower Na$^+$ diffusion barrier and the better stability of the SEI.[42] The polymeric nature of the SEI as seen from the SEM images indicates also a structural flexibility, which is a critical parameter for electrode reactions involving large volume changes. Changes in the electrode thickness during cycling are discussed in the following section.

2.4. In Situ Electrochemical Dilatometry

Considering the large theoretical volume expansion upon full sodiation of Sn and P (420% for formation of Na$_{14}$Sn$_4$ and 490% for Na$_3$P) the use of these compounds as bulk phases is unrealistic as cycling would lead to contact losses and electrode pulverization. Dispersing the active material in conductive carbon matrixes is an effective strategy to buffer the effective volume changes at the electrode level as already demonstrated for several alloying and conversion-type electrodes[1g] containing Si,[60] Sn,[17] or SnSb.[36]

To get insights on the volume changes experienced by the electrode upon cycling, the change of the electrode thickness upon cycling has been investigated using in situ electrochemical dilatometry (ECD). Results obtained for "Sn_4P_3"/NHC and Sn_4P_3 electrodes cycled in diglyme are displayed in **Figure 7** and Figure S10 (Supporting Information). While the capacities measured upon cycling of the in situ ECD cells did not match those recorded with coin cells, due to the rather different cell set-up, including a much larger thickness of the electrolyte, the thickness and voltage profiles are clearly correlated (compare panel a with c and b with d in Figure 7). The large initial thickness increase experienced by the "Sn_4P_3"/NHC (Figure 7a) and Sn_4P_3 (Figure 7b) electrodes is most likely associated with the rearrangement of particles along with SEI formation. Despite the large volume expansion for Sn_4P_3 at the material level, the effective volume change at the electrode level is much smaller. For the Sn_4P_3 electrode, the effective thickness change is the
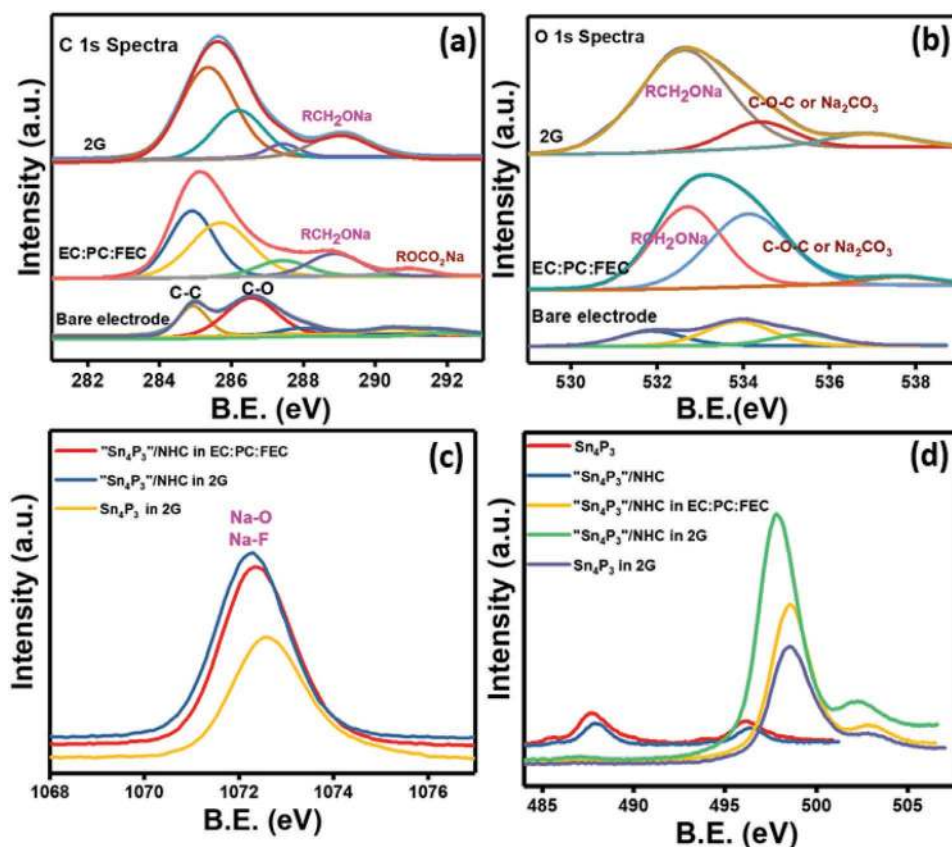
**ADVANCED
SCIENCE NEWS**

www.advancedsciencenews.com

**ADVANCED
FUNCTIONAL
MATERIALS**

www.afm-journal.de

Figure 6. a) Comparison of C 1s spectra b) O 1s spectra c) Na 1s spectra d) Sn 3d spectra of "Sn$_4$P$_3$"/NHC and Sn$_4$P$_3$ electrodes cycled in diglyme and EC:PC:FEC electrolytes.
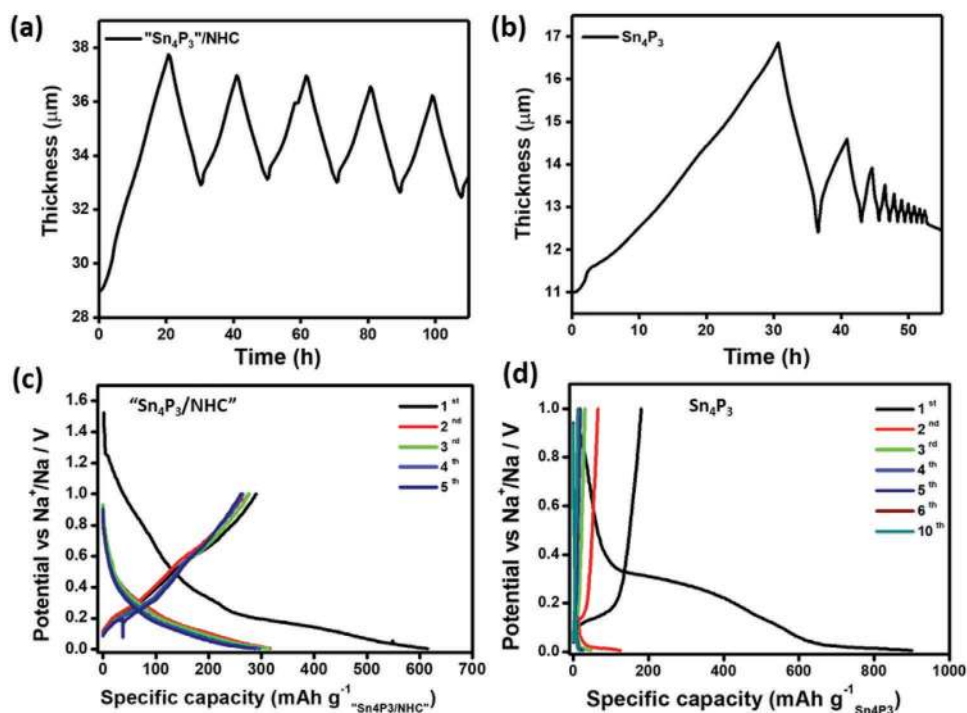

Figure 7. In situ ECD measurements at 50 mA g^{-1} over 50 h of consecutive cycling for a) five cycles for "Sn$_4$P$_3$"/NHC and b) 10 cycles for Sn$_4$P$_3$. c,d) Corresponding charge–discharge curves of "Sn$_4$P$_3$/NHC" and Sn$_4$P$_3$, respectively. (electrolyte-1 M NaPF$_6$ in diglyme).

range of 11–16.8 µm (first cycle), which corresponds to an increase of about ≈53%. Cycling of Sn_4P_3 was hardly possibly and rapid aging took place. For the "Sn_4P_3"/NHC electrode, the average absolute "breathing" of the electrode (second to fourth cycle) is around 4 µm, i.e., the electrode expands around 12% during sodiation (or 14% related to the initial thickness of 29 µm). The use of NHC reduces the relative expansion and improves cycle life, leading to a fairly reversible stability during cycling. It is worth noting that the "Sn_4P_3"/NHC electrodes investigated in this study have an active mass loading in the range of 1.4–1.7 mg cm^{-2}, corresponding to an areal capacity in the range of 0.72–0.74 mAh cm^{-2}. Such values are typical for many academic studies because of the nonoptimized electrode formulation and preparation. These are also very relevant to reduce the first cycle ICE, which is related to the large amount of carbon employed in the electrode.

2.5. In Situ XRD

The sodium storage mechanism has been studied by in situ XRD. Results are shown in **Figure 8**a and Figure S11 (Supporting Information). The voltage profiles obtained with the in situ cell nearly match the ones obtained with coin cells (Figure S12, Supporting Information). At open circuit voltage (OCV) conditions, the composite electrode shows clear reflections of Sn_4P_3 and Sn. After sodiation (at 0.005 V), the reflections corresponding

to Sn_4P_3 and Sn at around 30.9°, 31.7°, and 32.3° disappeared, while some peaks of $Na_{15}Sn_4$ (32.1°, 33.4°, 35.1°, and 37.6°, Reference code: 04-004-8571)[61] appeared through the formation of other intermetallic compounds of Na-Sn (e.g., Na–Sn, Na–Sn$_5$, Na$_9$Sn$_4$), (Figure 8a and Figure S11, Supporting Information). On the other hand, the reflections for sodiated compounds of phosphorous (e.g., Na$_3$P) were expected to appear at 36.1° and 37.0°[62] (Reference code: 04-011-9527),[63] however, their reflection is rather weak and a clear assignment is difficult (see Figure 8b). This is not surprising since conversion reactions in general lead to an amorphous matrix of sodium phosphides, oxides, or fluorides of the corresponding starting compound.[64] Recent NMR studies by Grey et al. provide evidence of Na$_3$P formation upon sodiation of black P in electrochemical cells.[62] As stated above that there is no clear evidence for the formation of Na$_3$P phases when discharging while we claim that Na$_3$P is formed to balance the electrochemical results. Overall, this suggests that sodiation of the electrode leads to the formation of Na$_{15}$Sn$_4$ and, possibly Na$_3$P, which are the end members of the ideal electrode reaction. When the electrode is then desodiated, the reflections corresponding to Na$_3$P and Na$_{15}$Sn$_4$ disappear. While ideally "Sn_4P_3" should reform during desodiation, the main reflections appearing correspond to Sn. This is in line with the capacity values, see Table S1 (Supporting Information). While almost full capacity is reached during first discharge, the capacity is lower during charging and the forthcoming cycles. Intermediate phases such as Na$_2$P, NaP, NaP$_5$, etc. may remain in the electrode yet these phases were not observed in the XRD pattern (most likely because of their amorphous nature).[65] In the second cycle, see Figure S13 (Supporting Information), the Sn reflections disappear along with appearance of again Na$_3$P and Na$_{15}$Sn$_4$. Subsequent desodiation then leads again to disappearance of Na$_3$P and Na$_{15}$Sn$_4$ along with formation of Sn (Figure 8a). Although no other charging product could be found by XRD, the results indicate that the electrode undergoes an activation in the first cycle, i.e., sodiation of Sn_4P_3 leads to formation of Na$_{15}$Sn$_4$ and Na$_3$P. During cycling, however, "Sn_4P_3" does not reform. Instead, Sn and (amorphous) P form during charging. Overall, the observed pathway matches the one previously suggested.[42–43,45]
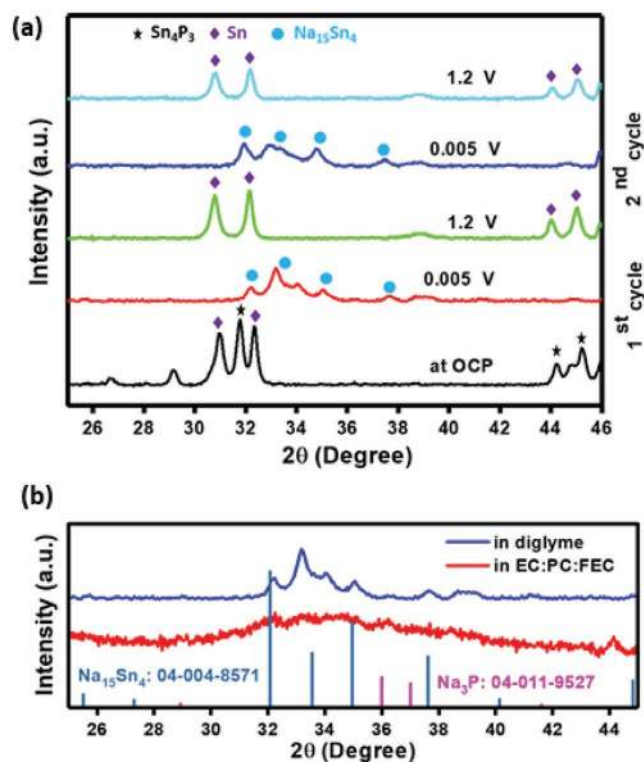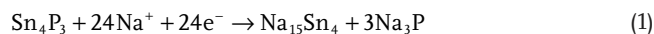
(Sodiation at the first cycle)

$$Sn_4P_3 + 24Na^+ + 24e^- \rightarrow Na_{15}Sn_4 + 3Na_3P \tag{1}$$

(sodiation/desodiation at the subsequent cycles)

$$Na_{15}Sn_4 \leftrightarrow 4Sn + 15Na^+ + 15e^- \tag{2}$$

$$Na_3P \leftrightarrow P + 3Na^+ + 3e^- \tag{3}$$

When changing the electrolyte solvent from diglyme to a EC:PC:FEC mixture, see Figure S14 (Supporting Information), the overall behavior is similar. However, reflections for Na$_{15}$Sn$_4$ and Na$_3$P at fully sodiated state (at 0.005 V versus Na$^+$/Na) and during desodiation were not as clearly observable as compared to the diglyme electrolyte (Figure 8b and Figure S14, Supporting Information).

Figure 8. a) In situ XRD patterns of "Sn_4P_3"/NHC measured at different potentials during sodiation and desodiation process in diglyme electrolyte. b) In situ XRD patterns of "Sn_4P_3"/NHC measured at 0.005 V versus Na$^+$/Na (at fully sodiated state) in diglyme and EC:PC:FEC electrolytes.

ADVANCED
SCIENCE NEWS
www.advancedsciencenews.com

ADVANCED
FUNCTIONAL
MATERIALS
www.afm-journal.de

3. Conclusion

A composite based on tin, phosphorous, and nitrogen doped hard carbon (NHC) with the formal composition "Sn_4P_3"/NHC (75:25 wt%) was prepared by a two-step ball milling process. In a first synthesis step, phase pure Sn_4P_3 was prepared from the elements by reactive ball-milling. In a second stage, the composite was prepared by milling Sn_4P_3 with NHC. During this step, Sn_4P_3 partly decomposes leading to a Sn and P (hence the notation "Sn_4P_3" instead of Sn_4P_3). The storage capacity in diglyme electrolytes was studied and compared with carbonate electrolytes with the former electrolyte leading to enhanced performance. The storage contributions of NHC (as well as the conductive additive Super P) to the electrode were deconvoluted and found to be below 10% suggesting that the major benefit of the carbon arises from embedding the Sn–P active phases thereby improving cycle life. In combination with the diglyme electrolyte this provides a capacity of 550 mAh $g_{electrode}^{-1}$ at 50 mA g^{-1} and 440 mAh $g_{electorde}^{-1}$ over 500 cycles (83% of capacity retention) being a notable improvement compared to previous studies. The structural stability of the conversion electrode is also rationalized using in situ electrochemical dilatometry, showing that the electrode "breathes" much less (12–14% @ 300 mAh g^{-1}) as compared to what would be expected from the bulk phase (490%) and the respective bulk electrode (53%). In situ XRD shows that the conversion reaction during initial discharge leads to $Na_{15}Sn_4$ and, possibly, Na_3P. However, the original phase mixture does not reform during charging. The products after charging are Sn and (amorphous) P. Overall, this study shows that the combination of "Sn_4P_3" phases with NHC as carbon matrix leads to high capacity combined with prolonged cycle life when using ether electrolytes.

4. Experimental Section

Synthesis of "Sn_4P_3"/NHC: Synthesis of "Sn_4P_3"/NHC was done by a two-step ball milling process. Initially Sn_4P_3 was prepared by milling of Sn (Alfa Aesar, 99.8% purity) and red phosphorous (P) (Sigma Aldrich, 99.9% purity) with the molar ratio of 4:3 for 24 h. Accordingly, Sn (1.6 g) and red P (313 mg) were mixed in zirconium oxide (ZrO_2) coated jar (60 mL) using a planetary ball mill from Fritsch. The mixture was mechanically milled for 24 h at 400 rpm with a ZrO_2 ball (8 mm diameter) to powder ratio of 20:1 under Ar atmosphere. Subsequently, the as-prepared Sn_4P_3 was mixed with nitrogen-doped hard carbon (NHC) in a 75:25 mass ratio in a ZrO_2 coated jar. The powder mixture was then ball-milled for 24 h under identical experimental conditions. NHC was prepared by annealing Chitosan (Sigma Aldrich) at 1100 °C by using a tubular furnace (Nabertherm GmbH) with a heating rate of 5 °C per min for 3 h in Ar atmosphere (mass flow-10 sccm). After pyrolysis, the resulting NHC was washed with ethanol and dried at 60 °C.

Material Characterizations: Transmission electron microscopy (TEM) characterization was carried out with a FEI Tecnai G2 FEG (operating at 200 kV) equipped with an X-MaxN 80T SDD EDXS system (Oxford). Samples for the TEM studies were prepared by dispersing the powdered sample onto a TEM lacey copper grid. EDX elemental maps were acquired in STEM mode with active drift compensation. XRD measurements were performed using a Bruker Phaser 2 diffractometer equipped with a Cu Kα source with 20 kV as operating voltage. Morphological investigations were carried out by using a SEM (Phenom ProX) operated at 15 kV accelerating voltage. XPS measurements were performed with a K-alpha Thermo Fisher Scientific spectrometer using a monochromatic Al Kα

source. Spectra were analyzed with a Thermo Avantage software. The electrode thickness was measured by a digital thickness dial gauge from Käfer Messuhrenfabrik GmbH. Ex situ XPS analysis was carried out in SPECS UHV system (FOCUS 500 monochromated X-ray source, PHOIBOS 150 hemispherical energy analyzer with 1D DLD detector) using the Al-Kα (1486.6 eV) radiation at a base pressure of 10^{-10} mbar. The measurements were performed using pass energies at the analyzer of 60 and 30 eV for survey and detail spectra, respectively. Electrodes were inserted into the XPS vacuum chamber by using an Ar-filled transfer system. The X-ray photoelectron spectra were calibrated to 284.6 eV (C–C/C–H bond in carbon super P) for all the spectra.

In situ XRD measurements were carried out on a Bruker D8 Advance diffractometer by using a home-made airtight stainless-steel cell equipped with a Be window.[66] The electrode slurry was prepared in 1-methylpyrrolidine by mixing with 80 wt% active material, 10 wt% carbon black Super C65 and 10 wt% PVdF and casted over a beryllium current collector and dried under vacuum at 120 °C overnight. Na metal was used as counter electrode and separated from working electrode using a Whatman GF/D glass fiber separator. The cell assembly was carried out in a moisture free glove box (H_2O < 0.5 ppm, O_2 < 0.3 ppm), and 1 M $NaPF_6$ in diglyme or EC:PC:FEC were used as the electrolyte. The electrode was continuously scanned in Bragg Brentano geometry between $2\theta = 25°$ to $80°$ during the charge and discharge at 0.05 A g^{-1}; one scan lasts for 20 min in both cases.

Electrochemical Measurements: The "Sn_4P_3"/NHC electrodes were fabricated by conventional slurry-based method. The active materials, the binder poly(vinylidene difluoride, PVdF), and the conductive additive super P carbon black were mixed with a mass ratio of 75:10:15 in N-methyl-2-pyrrolidone (NMP) until a homogeneous slurry was obtained. Then, the slurry was casted onto Cu foil (carbon-coated) and dried for 12 h under vacuum at 105 °C. 12 mm diameter electrodes where punched by using a punching machine. The active mass loading was in the range of 1.4–1.7 mg cm^{-2}. The coin cells (CR2032 Coin Cells by MTI Corp.) were assembled using "Sn_4P_3"/NHC as an active anode material and sodium metal (BASF SE Corporation) as counter electrode in two-electrode cells inside an argon-filled glove box (<0.1 ppm O_2 and H_2O). A 1 M solution of sodium hexafluorophosphate ($NaPF_6$, Sigma Aldrich) in diethylene glycol dimethyl ether (diglyme, anhydrous purity >99.5%, Sigma Aldrich) was used as the electrolyte (150 µL). Whatman glass microfiber filters (GF/A) were used as the separator. For comparison, a solution of $NaPF_6$ (1 M) in ethylene carbonate (EC)/ propylene carbonate (PC) (1:1 vol ratio) was used as a reference system. Fluoroethylene carbonate (FEC) (2% volume) was also used as the additive for carbonate-based electrolytes. The cells were tested by using a Biologic BCS cycler at 25 °C. The cells were galvanostatically charged and discharged at various current densities from 50 mA g^{-1} to 2 A g^{-1} in the voltage range 0.005 to 1.0 V versus Na^+/Na. Electrochemical impedance spectroscopy (EIS) measurements were performed in a two-electrode cell using a SP 200 device from Biologic in the frequency range of 1 MHz to 10 mHz with an amplitude of 10 mV.

Supporting Information

Supporting Information is available from the Wiley Online Library or from the author.

Conflict of Interest

The authors declare no conflict of interest.

Keywords

[1] a) H. Pan, Y. S. Hu, L. Chen, *Energy Environ. Sci.* **2013**, *6*, 2338; b) V. Palomares, P. Serras, I. Villaluenga, K. B. Hueso, J. C. Gonzalez, T. Rojo, *Energy Environ. Sci.* **2012**, *5*, 5884; c) N. Yabuuchi, K. Kubota, M. Dahbi, S. Komaba, *Chem. Rev.* **2014**, *114*, 11636; d) P. K. Nayak, L. Yang, W. Brehm, P. Adelhelm, *Angew. Chem., Int. Ed.* **2018**, *57*, 102; e) J. Y. Hwang, S. T. Myung, Y. K. Sun, *Chem. Soc. Rev.* **2017**, *46*, 3529; f) M. D. Slater, D. Kim, E. Lee, C. S. Johnson, *Adv. Funct. Mater.* **2013**, *23*, 947; g) H. Zhang, I. Hasa, S. Passerini, *Adv. Energy Mater.* **2018**, *8*, 1702582; h) T. Placke, R. Kloepsch, S. Duehnen, M. Winter, *J. Solid State Electrochem.* **2017**, *21*, 1939.

[2] a) O. Lenchuk, P. Adelhelm, D. Mollenhauer, *Phys. Chem. Chem. Phys.* **2019**, *21*, 19378; b) Y. Li, Y. Lu, P. Adelhelm, M. M. Titirici, Y. S. Hu, *Chem. Soc. Rev.* **2019**, *48*, 4655.

[3] B. Jache, P. Adelhelm, *Angew. Chem., Int. Ed.* **2014**, *53*, 10169.

[4] I. Hasa, X. Dou, D. Buchholz, Y. S. Horn, J. Hassoun, S. Passerini, B. Scrosati, *J. Power Sources* **2016**, *310*, 26.

[5] X. Dou, I Hasa, D. Saurel, C. Vaalma, L. Wu, D. Buchholz, D. Bresser, S. Komaba, S. Passerini, *Mater. Today* **2019**, *23*, 87.

[6] S. Wenzel, T. Hara, J. Janek, P. Adelhelm, *Energy Environ. Sci.* **2011**, *4*, 3342.

[7] R. Alcantara, J. M. J. Mateos, J. L. Tirado, *J. Electrochem. Soc.* **2002**, *149*, 201.

[8] Y. Li, L. Mu, Y. S. Hu, H. Li, L. Chen, X. Huang, *Energy Storage Mater.* **2016**, *2*, 139.

[9] D. Stevens, J. Dahn, *J. Electrochem. Soc.* **2000**, *147*, 1271.

[10] S. Komaba, W. Murata, T. Ishikawa, N. Yabuuchi, T. Ozeki, T. Nakayama, A. Ogata, K. Gotoh, K. Fujiwara, *Adv. Funct. Mater.* **2011**, *21*, 3859.

[11] a) Z. Li, Z. Jian, X. Wang, I. A. Rodrıguez-Perez, C. Bommier, X. Ji, *Chem. Commun.* **2017**, *53*, 2610; b) K. Wang, Y. Jin, S. Sun, Y. Huang, J. Peng, J. Luo, Q. Zhang, Y. Qiu, C. Fang, J. Han, *ACS Omega* **2017**, *2*, 1687; c) V. Simone, A. Boulineau, A. de Geyer, D. Rouchon, L. Simonin, S. Martinet, *J. Energy Chem.* **2016**, *25*, 761.

[12] P. Thomas, D. Billaud, *Electrochim. Acta* **2001**, *46*, 3359.

[13] S. Wun, R. Ge, M. Lu, R. Xu, Z. Zhang, *Nano Energy* **2015**, *15*, 379.

[14] C. Bommier, T. W. Surta, M. Dolgos, X. Ji, *Nano Lett.* **2015**, *15*, 5888.

[15] E. M. Lotfabad, J. Ding, K. Cui, A. Kohandehghan, W. P. Kalisvaart, M. Hazelton, D. Mitlin, *ACS Nano8*, 7115.

[16] Q. Meng, Y. Lu, F. Ding, Q. Zhang, L. Chen, Y. S. Hu, *ACS Energy Lett.* **2019**, *4*, 2608.

[17] T. Palaniselvam, M. Goktas, B. Anothumakkool, Y. N. Sun, R. Schmuch, L. Zhao, B. H. Han, M. Winter, P. Adelhelm, *Adv. Funct. Mater.* **2019**, *29*, 1900790.

[18] a) S. Komaba, Y. Matsuura, T. Ishikawa, N. Yabuuchi, W. Murata, S. Kuze, *Electrochem. Commun.* **2012**, *21*, 65; b) Z. Li, J. Ding, D. Mitlin, *Acc. Chem. Res.* **2015**, *48*, 1657; c) Y. Xu, Y. Zhu, Y. Liu, C. Wang, *Adv. Energy Mater.* **2013**, *3*, 128; d) C. Kim, K. Y. Lee, I. Kim, J. Park, G. Cho, K. W. Kim, J. H. Ahn, H. J. Ahn, *J. Power Sources* **2016**, *317*, 153; e) Y. Liu, N. Zhang, L. Jiao, Z. Tao, J. Chen, *Adv.*

[19] a) M. Lao, Y. Zhang, W. Luo, Q. Yan, W. Sun, S. X. Dou, *Adv. Mater.* **2017**, *29*, 1700622; b) L. D. Ellis, T. D. Hatchard, M. N. Obrovac, *J. Electrochem. Soc.* **2012**, *159*, 1801.

[20] a) N. Yabuuchi, Y. Matsuura, T. Ishikawa, S. Kuze, J. Y. Son, Y. T. Cui, H. Oji, S. Komaba, *ChemElectroChem* **2014**, *1*, 580; b) W. L. H. X. Li Jiaoyang, *Prog. Chem.* **2016**, *28*, 193; c) B. Peng, Y. Xu, K. Liu, X. Wang, F. M. Mulder, *ChemElectroChem* **2017**, *4*, 2140; d) G. L. Xu, Z. Chen, G. M. Zhong, Y. Liu, Y. Yang, T. Ma, Y. Ren, X. Zuo, X. H. Wu, X. Zhang, K. Amine, *Nano Lett.* **2016**, *16*, 3955; e) S. Liu, J. Feng, X. Bian, J. Liu, H. Xu, Y. An, *Energy Environ. Sci.* **2017**, *10*, 1222; f) Y. Zhu, Y. Wen, X. Fan, T. Gao, F. Han, C. Luo, S. C. Liou, C. Wang, *ACS Nano* **2015**, *9*, 3254; g) J. Zhou, X. Liu, W. Cai, Y. Zhu, J. Liang, K. Zhang, Y. Lan, Z. Jiang, G. Wang, Y. Qian, *Adv. Mater.* **2017**, *125*, 1700214.

[21] a) Y. Kim, Y. Park, A. Choi, N. S. Choi, J. Kim, J. Lee, J. H. Ryu, S. M. Oh, K. T. Lee, *Adv. Mater.* **2013**, *25*, 3045; b) W. J. Li, S. L. Chou, J. Z. Wang, H. K. Liu, S. X. Dou, *Nano Lett.* **2013**, *13*, 5480; c) Y. Liu, N. Zhang, L. Jiao, J. Chen, *Adv. Mater.* **2015**, *27*, 6702.

[22] J. Choi, W. S. Kim, K. H. Kim, S. H. Hong, *J. Mater. Chem. A* **2018**, *6*, 17437.

[23] J. W. Wang, X. H. Liu, S. X. Mao, J. Y. Huang, *Nano Lett.* **2012**, *12*, 5897.

[24] J. Qian, X. Wu, Y. Cao, X. Ai, H. Yang, *Angew. Chem.* **2013**, *125*, 4731.

[25] J. Liu, P. Kopold, C. Wu, P. A. V Aken, J. Maier, Y. Yu, *Energy Environ. Sci.* **2015**, *8*, 3531.

[26] W. Li, S. Hu, X. Luo, Z. Li, X. Sun, M. Li, F. Liu, Y. Yu, *Adv. Mater.* **2017**, *29*, 1605820.

[27] M. Sha, H. Zhang, Y. Nie, K. Nie, X. Lv, N. Sun, X. Xie, Y. Ma, X. Sun, *J. Mater. Chem. A* **2017**, *5*, 6277.

[28] W. Wang, J. Zhang, D. Y. W Yu, Q. Li, *J. Power Sources* **2017**, *364*, 420.

[29] A. Ponrouch, A. R. Goni, M. R. Palacin, *Electrochem. Commun.* **2013**, *27*, 85.

[30] J. Qian, X. Wu, Y. Cao, X. Ai, H. Yang, *Angew. Chem., Int. Ed.* **2013**, *52*, 4633.

[31] H. Usui, T. Sakata, M. Shimizu, H. Sakaguchi, *Electrochemistry* **2015**, *83*, 810.

[32] M. Goktas, C. Bolli, E. J. Berg, P. Novak, K. Pollok, F. Langenhorst, M. v. Roeder, O. Lenchuk, D. Mollenhauer, P. Adelhelm, *Adv. Energy Mater.* **2018**, *8*, 1702724.

[33] K. Westman, R. Dugas, P. Jankowski, W. Wieczorek, G. Gachot, M. Morcrette, E. Irisarri, A. Ponrouch, M. R. Palacin, J. M. Tarascon, P. Johansson, *ACS Appl. Energy Mater.* **2018**, *1*, 2671.

[34] C. Wang, D. Du, M. Song, Y. Wang, F. Li, *Adv. Energy Mater.* **2019**, *9*, 1900022.

[35] K. Lei, C. Wang, L. Liu, Y. Luo, C. Mu, F. Li, J. Chen, *Angew. Chem., Int. Ed.* **2018**, *57*, 4687.

[36] W. Brehm, J. R. Buchheim, P. Adelhelm, *Energy Technol.* **2019**, *7*, 1900389.

[37] B. Zhang, G. Rousse, D. Foix, R. Dugas, D. A. D. Corte, J. M. Tarascon, *Adv. Mater.* **2016**, *28*, 9824.

[38] M. Goktas, C. Bolli, J. Buchheim, E. J. Berg, P. Novak, F. Bonilla, T. Rojo, S. Komaba, K. Kubota, P. Adelhelm, *ACS Appl. Mater. Interfaces* **2019**, *11*, 32844.

[39] J. L. G. Camer, B. Acebedo, N. O. Vitoriano, I. Monterrubio, M. Galceran, T. Rojo, *J. Mater. Chem. A* **2019**, *7*, 18434.

[40] S. K. Das, B. Jache, H. Lahon, C. L. Bender, J. Janek, P. Adelhelm, *Chem. Commun.* **2016**, *52*, 1428.

[41] K. Li, J. Zhang, D. Lin, D. W. Wang, B. Li, W. Lv, S. Sun, Y. B. He, F. Kang, Q. H. Yang, L. Zhou, T. Y. Zhang, *Nat. Commun.* **2019**, *10*, 725.

**ADVANCED
SCIENCE NEWS**

www.advancedsciencenews.com

**ADVANCED
FUNCTIONAL
MATERIALS**

www.afm-journal.de

[42] J. Qian, Y. Xiong, Y. Cao, X. Ai, H. Yang, *Nano Lett.* **2014**, *14*, 1865.

[43] Y. Xu, B. Peng, F. M. Mulder, *Adv. Energy Mater.* **2018**, *8*, 1701847.

[44] L. Zheng, R. A. Dunlap, M. N. Obrovac, *J. Electrochem. Soc.* **2016**, *163*, 1188.

[45] W. Li, S. L. Chou, J. Z. Wang, J. H. Kim, H. K. Liu, S. X. Dou, *Adv. Mater.* **2014**, *26*, 4037.

[46] X. M. Lin, J. H. Chen, J. J. Fan, Y. Ma, P. Radjenovic, Q. C. Xu, L. Huang, S. Passerini, Z. Q. Tian, J. F. Li, *Adv. Energy Mater.* **2019**, *9*, 1902312.

[47] a) A. Mehmood, G. Alic, B. Koyutürk, J. Pampel, K. Y. Chung, T. P. Fellinger, *Energy Storage Mater.* **2020**, *28*, 101; b) N. Wang, Q. Liu, B. Sun, J. Gu, B. Yu, W. Zhang, D. Zhang, *Sci. Rep.* **2018**, *8*, 9934.

[48] W. Zhang, J. Mao, S. Li, Z. Chen, Z Guo, *J. Am. Chem. Soc.* **2017**, *139*, 3316.

[49] W. Li, Z. Yang, Y. Jiang, Z. Yu, L. Gu, Y. Yu, *Carbon* **2014**, *78*, 455.

[50] a) H. L. Su, Y. Xie, B. Li, X. M. Liu, Y. T. Qian, *J. Solid State Chem.* **1999**, *146*, 110; b) O. Olofsson, *Acta Chem. Scand.* **1970**, *24*, 1153.

[51] J. Liu, S. Wang, K. Kravchyk, M. Ibanez, F. Krumeich, R. Widmer, D. Nasiou, M. Meyns, J. Llorca, J. Arbiol, M. V. Kovalenko, A. Cabot, *J. Mater. Chem. A* **2018**, *6*, 10958.

[52] V. Tallapally, R. J. A. Esteves, L. Nahar, I. U. Arachchige, *Chem. Mater.* **2016**, *28*, 5406.

[53] X. Yan, Y. Yu, X. Yang, *RSC Adv.* **2014**, *4*, 24986.

[54] M. H. Mobarok, E. J. Luber, G. M. Bernard, L. Peng, R. E. Wasylishen, J. M. Buriak, *Chem. Mater.* **2014**, *26*, 1925.

[55] J. Zhang, D. W. Wang, W. Lv, S. Zhang, Q. Liang, D. Zheng, F. Kang, Q. H. Yang, *Energy Environ. Sci.* **2017**, *10*, 370.

[56] S. Komaba, T. Ishikawa, N. Yabuuchi, W. Murata, A. Ito, Y. Ohsawa, *ACS Appl. Mater. Interfaces* **2011**, *3*, 4165.

[57] F. Klein, R. Pinedo, P. Hering, A. Polity, J. Janek, P. Adelhelm, *J. Phys. Chem. C* **2016**, *120*, 1400.

[58] C. C. Wang, L. B. Wang, F. J. Li, F. Y. Cheng, J. Chen, *Adv. Mater.* **2017**, *29*, 1702212.

[59] D. W. Su, K. Kretschmer, G. X. Wang, *Adv. Energy Mater.* **2016**, *6*, 1501785.

[60] J. L. G. Camer, C. Bünzli, M. M. Hantel, T. Poux, P. Novak, *Carbon* **2016**, *105*, 42.

[61] W. Midler, K. Volk, *Z. Naturforsch.* **1978**, *33*, 275.

[62] L. E. Marbella, M. L. Evans, M. F. Groh, J. Nelson, K. J. Griffith, A. J. Morris, C. P. Grey, *J. Am. Chem. Soc.* **2018**, *140*, 7994.

[63] a) Y. Dong, F. J. DiSalvo, *Acta Crystallogr., Sect. E: Crystallogr. Commun.* **2005**, *61*, 223. b) S. Kaushika, K. Matsumoto, Y. Sato, R. Hagiwara, *Electrochem. Commun.* **2019**, *102*, 46.

[64] F. Klein, B. Jache, A. Bhide, P. Adelhelm, *Phys. Chem. Chem. Phys.* **2013**, *15*, 15876.

[65] J. Sottmann, M. D. Michiel, H. Fjellvag, L. Malavasi, S. Margadonna, P. Vajeeston, G. B. M. Vaughan, D. S. Wragg, *Angew. Chem., Int. Ed.* **2017**, *56*, 11385.

[66] D. Bresser, E. Paillard, R. Kloepsch, S. Krueger, M. Fiedler, R. Schmitz, D. Baither, M Winter, S. Passerini, *Adv. Energy Mater.* **2013**, *3*, 513.